Predicting predawn leaf water potential while accounting for uncertainty using vine shoot growth and weather data in Mediterranean rainfed vineyards

Yulin Zhang, Léo Pichon, Anne Pellegrino, Sébastien Roux, Cécile Péruzzaro, Bruno Tisseyre

HAL Id: hal-04678463
https://hal.inrae.fr/hal-04678463v1

Submitted on 27 Aug 2024

Predicting predawn leaf water potential while accounting for uncertainty using vine shoot growth and weather data in Mediterranean rainfed vineyards

Yulin Zhang [a,*], Léo Pichon [a], Anne Pellegrino [b], Sébastien Roux [c], Cécile Péruzzaro [a], Bruno Tisseyre [a]

[a] *ITAP, Univ Montpellier, INRAE, Institut Agro, 2 Place Pierre Viala, Montpellier 34060, France*
[b] *LEPSE, Univ Montpellier, INRAE, Institut Agro, 2 Place Pierre Viala, Montpellier 34060, France*
[c] *MISTEA, Univ Montpellier, INRAE, Institut Agro, 2 Place Pierre Viala, Montpellier 34060, France*

ARTICLE INFO

ABSTRACT

Monitoring vine water status is crucial for wine production. However, in Mediterranean regions, a key indicator for evaluating this information, predawn leaf water potential (Ψpd), is challenging to obtain in terms of logistics and costs. To address this, the iG-Apex, a plant growth index based on vine shoot growth observations has been proposed as being both low-cost and easy to collect. It has been found that a strong correlation exists between iG-Apex and Ψpd. Nonetheless, the relationship between iG-Apex and Ψpd becomes increasingly uncertain as the growing season progresses. Therefore, while being operationally attempting, modeling Ψpd from iG-Apex necessitates the consideration of prediction uncertainty. This study presents a modeling approach, named the Recursive-Duo-Model (RDM), which integrates predictive modeling and Bayesian resampling to estimate Ψpd with iG-Apex while reducing prediction uncertainty. Using iG-Apex and readily accessible weather data, the RDM aims to reduce the cost to obtain the key indicator for monitoring vine water status. The study evaluated the RDM's performance across four water deficit scenarios: no deficit (-0.3 ≤ observed Ψpd < 0 MPa), mild to moderate deficit (-0.5 ≤ observed Ψpd < −0.3 MPa), moderate to severe deficit (-0.8 ≤ observed Ψpd < −0.5 MPa), and high deficit (observed Ψpd ≤ −0.8 MPa). Results showed satisfactory prediction accuracy (R^2=0.61, RMSE=0.14 MPa), with the method effectively detecting the first three water deficit scenarios. In parallel, the RDM reduced prediction uncertainty (mean width of 80 % confidence interval=0.20 MPa) compared to a conventional approach based solely on vine shoot growth data (mean width=0.36 MPa).

1. Introduction

Monitoring vine water status is an essential practice in vineyard management (Deloire et al., 2020). This parameter significantly affects leaf area hence light interception (Albrizio et al., 2023), fruit yield (Laurent et al., 2021), and wine quality (Xi et al., 2010). In regions with hot and dry summer, like the Mediterranean basin (Baeza et al., 2007), Predawn Leaf Water Potential (Ψpd) is considered as a robust indicator of vine water status (Choné et al., 2001). This indicator is commonly used as the reference to calibrate other water status indicators for precision irrigation (García-Tejera et al., 2021). However, measuring Ψpd involves major logistical constraints (e.g. nocturnal measurements), and requires specific materials (e.g. pressure chamber) (Scholander et al.,

1965). Consequently, although this approach is reliable, collecting Ψpd measurements is therefore challenging in practice.

Multiple studies have investigated alternative approaches for estimating vine water status, for replacing the high-labor Ψpd acquisition (Rienth and Scholasch, 2019). For example, Acevedo-Opazo et al. (2010a) suggested estimating Ψpd at multiple sites from the Ψpd measured at one reference site through a locally calibrated spatially extrapolation model. However, this approach requires heavy Ψpd data acquisition for the model calibration. Other authors proposed to estimate Ψpd using a mechanistic model (Celette et al., 2010), which depends on a high number of model parameters. Wallach et al. (2014) have shown that an accurate parameterization is a prerequisite for these models to generate meaningful predictions, but obtaining parameters

necessitates a huge amount of work. In the recent years, many researchers have been trying to model Ψpd using machine learning algorithms from other more accessible data. These data-driven approaches have been mostly focusing on spectral reflectance data (Romero et al., 2018; Tosin et al., 2021). Yet, acquiring this data is still costly, since it requires specific skills, expensive materials, and the data collection may be influenced by weather condition (Pôças et al., 2015). Despite the interest of these approaches, their practical limitations make them not suitable enough for monitoring vine water status in commercial vineyards, especially for small-farm holders.

An alternative approach for assessing vine water status was proposed by Pichon et al. (2021), based on a vine shoot growth index named iG-Apex. Relying on visual observations of vine shoots, the iG-Apex measurement is easy to collect in field (less than 5 minutes per measurement). By using a free mobile application (Brunel et al., 2019), the index can be conveniently obtained using a standardized protocol. More interestingly, it has been demonstrated that a strong correlation exists between iG-Apex and Ψpd when the latter varies between −0.2 and −0.8 MPa, showing a quasi-linear relationship (Pichon et al., 2023). Nevertheless, this index has several limitations that restrict its operational use. Firstly, as water deficit intensifies, the uncertainty in the relation between iG-Apex and Ψpd increases (Pichon et al., 2023). Secondly, beyond a certain level of water deficit, all apexes stop their vegetative growth, thus, a variation in Ψpd does not lead to any change in iG-Apex anymore. Lastly, there is a time lag between the plant's actual water status and the information provided by iG-Apex (Pellegrino et al., 2005), which reacts with a latency towards Ψpd variation. Although the relationship between Ψpd and iG-Apex has been known to be uncertain, this uncertainty is poorly described in the literature. Additionally, in general, prediction uncertainty has been overlooked in current Ψpd modeling projects (Tosin et al., 2022), even though uncertainty information has been proven to be important for vinegrowers in water stress management (Roux et al., 2014).

Bayesian modeling provides a complete toolset to account for uncertainty (Khanal et al., 2019; Kocian et al., 2020; Chang et al., 2023). The approach considers the searched quantity as a random variable and represents it as a distribution (McElreath, 2016). This allows end users to consider multiple most probable scenarios when no single best estimation could be made. More specifically, Gordon et al. (1993) proposed a Bayesian recursive algorithm, which modifies a prior distribution in order to obtain a less uncertain posterior distribution. This process is called Bayesian resampling (Kuptametee and Aunsri, 2022). For operational concerns, it should be beneficial not only to provide a realistic description of the uncertainty associated to Ψpd predictions, but also to reduce this uncertainty for end-users in order to facilitate their decision, as shown by Acevedo-Opazo et al. (2010b).

Nonetheless, the resampling approach has never been integrated in Ψpd prediction. The main difficulty is that by construction, the algorithm requires a dynamic model which simulates the evolution of Ψpd, and/or an actually observed Ψpd, both serving to modify prior distributions. In practice, both elements are difficult to obtain. However, an actual Ψpd observation could be replaced by a value predicted by machine learning algorithms from relevant information. For instance, weather data is an easily accessible type of data, which has been used to model Ψpd with a regression model under non-irrigated conditions (Taylor et al., 2012). This data quantifies the climatic demand, and have the advantage to describe short-term Ψpd variations without the latency observed in iG-Apex (Pellegrino et al., 2006). Additionally, like many other agronomic variables (e.g. leaf area index, plant height), Ψpd is auto-correlated over time. That means knowing the level of previous Ψpd level should help estimating the current one (Pôças et al., 2020).

The objective of this study is to combine machine learning and Bayesian resampling approach for modeling Ψpd from iG-Apex, while quantifying and reducing its uncertainty. The proposed approach deployed time series of vine shoot growth and weather data, as well as an algorithm that accounts for Ψpd's auto-correlation over time. The underlying hypothesis was that the tested method will not only improve the accuracy of predictions, but also reduce their uncertainty compared to a more conventional approach of predicting Ψpd using iG-Apex alone.

2. Materials and methods

2.1. Experimental sites

Two experimental sites were studied in southern France, Occitanie region (Fig. 1a) to account for different soil conditions. Both sites were rainfed. The first site was the vineyard of Tavel, in the southern Rhône Valley (WGS84: 44.009484°N, 4.682064°E) (Fig. 1b). The vineyard covers over 900 ha. The texture of soil in the studied zone was mainly sandy-clay. The climate was Mediterranean, characterized by hot and dry summers (Luterbacher et al., 2012). This site included 33 measurement plots, with each plot consisting of 10 consecutive vines along a row. The second site was the "Domaine du Chapitre", 10 km south of Montpellier and 4 km north of coast (WGS84: 43.532103°N, 3.863947°E) (Fig. 1c). The area of this vineyard was 35 ha. The soil texture was mainly between silty-clay and clay. The climate was also Mediterranean. There were 12 measurement plots monitored, each containing 10 consecutive vines evenly distributed across two neighboring rows (5 vines per row). In both sites, vines training method was characterized by vertical shoot positioning with 3 levels of trellising. The experiment included two grape cultivars of *Vitis vinifera*: cv. Grenache for the Tavel site, and cv. Syrah for "Domaine du Chapitre". In both sites, the main limiting factor of vine growth was related to water deficit.

2.2. Raw data acquisition

Three types of raw data were collected prior to model training: predawn leaf water potential (Ψpd), vine shoot growth observations (iG-Apex), and weather variables.

2.2.1. Predawn leaf water potential

Ψpd was measured between 3 a.m. and 5 a.m. using a pressure chamber (Scholander et al., 1965). Among 10 vines in each measurement plot, 5 mature, non-senescing vines were identified, registered, and marked in fields. The choice of vines was made by selecting plants which were not impacted by diseases or anomalies at the beginning of the growing season. Each measurement was realized on a fully developed and healthy leaf located at the middle of a shoot. The same protocol was repeated on all 5 registered vines in each plot. Ψpd of a given plot for a given date was calculated by averaging the 5 measurements. The operator was chosen intentionally to be the same person to limit operator effect (Levin, 2019). Ψpd was monitored weekly in each measurement plot (from June 1st to September 5th). Five growing seasons were studied in the Tavel site (years 2008–2012), and one in "Domaine du Chapitre" (year 2022).

2.2.2. Vine shoot growth index: iG-Apex

Vine shoot growth was evaluated using the iG-Apex index as proposed by Pichon et al., (2021). Data were collected with the smartphone application ApeX-Vigne (Brunel et al., 2019). In each measurement plot, 50 vine shoots (5 per vines) were observed and classified by an operator into three categories: (a) full growth, (b) moderate growth, and (c) stopped growth. The iG-Apex was calculated as an average of weights attributed to these 50 observed vine shoots. The weights are 1, 0.5, or 0, depending on whether each observed vine shoot is classified as category (a), (b), or (c). In both experimental sites, the operator was chosen intentionally to be the same person to limit operator effect (Pichon et al., 2023). The iG-Apex indicator was always measured at the same date and in the same measurement plots as Ψpd, forming pairs of iG-Apex and Ψpd observations. These pairs measured at different dates gave iG-Apex and Ψpd time series, containing at least 3, and in average 7 observations per site and per year.

Fig. 1. (a) General location of two experimental sites. Detailed location of monitored plots (red dots) in (b) Tavel and (c) "Domaine du Chapitre".

2.2.3. Weather data

SAFRAN (translation from French: analysis system providing information for avalanche hazard) weather data of the two experimental sites were provided by Météo-France. They were downloaded via the SICLIMA platform developed by AgroClim-INRAE. This data source was the reference for hydrological monitoring throughout the metropolitan France. According to Taylor et al. (2012), four types of weather data were extracted at the daily frequency: temperature (including daily mean, minimum, and maximum value), relative humidity, precipitation, and potential evapo-transpiration calculated from the Penman-Monteith equation (Allen et al., 1989). For all measurement plots of each experimental site, weather conditions were considered as uniform.

2.2.4. Summary of raw datasets

The dataset from Tavel contained 409 pairs of iG-Apex and Ψpd observations collected from 2008 to 2012, consisting of 70 time series. The dataset from "Domaine du Chapitre" contained 144 pairs of observations collected in 2022, containing 12 time series.

2.3. Predictors and training data

Before model training, feature engineering was realized to extract predictors from raw data. All predictors are presented in Table 1.

2.3.1. Predictors related to iG-Apex observations

In order to account for both iG-Apex observations and temporal dynamic of iG-Apex, several predictors were derived from time series data: iG-Apex observations (noted *a*), variation of iG-Apex between two observations (*da*) and number of days between two observations (*diff_day*). By construction, *da* and *diff_day* were not available for the first observation of each time series.

Other predictors were derived to account for the general trend of iG-Apex time series and change in water deficit experienced by the vines. This general trend was modeled using a logistic regression (Lebon et al., 2006).

$$[iG - Apex]_t = \frac{1}{1 + e^{-k(x0-t)}} + \varepsilon \tag{1}$$

Where *t* stands for the day of the year, *x*0 for the inflection point of the curve, *k* for the slope at inflexion point, and ε represents the error of the model.

Two parameters *x*0 and *k*, derived from the logistic regression, were used as predictors. Along measurements during each season, these two parameter values were re-estimated at each time when a new iG-Apex value was available. Given that fitting the logistic regression requires at least 3 observations, the parameter values were not available for the first 2 data points in each time series.

2.3.2. Predictors related to weather data

Common daily weather variables were used as predictors, as proposed by Taylor et al. (2012): the minimum and maximum daily temperature (respectively T_{min} and T_{max}), the relative humidity of the day (*RH*), and the daily potential evapotranspiration (*ET0*). Other weather-related predictors were also inspired by their work. For instance, in order to account for effective impact of temperature on vine growth, Growing Degree Day (*GDD*) was calculated.

$$GDD = \begin{cases} T_{mean} - T_{base} & T_{mean} - T_{base} \geq 0 \\ 0 & T_{mean} - T_{base} < 0 \end{cases} \tag{2}$$

where $T_{base} = 10\ °C$ (Winkler et al., 1974), and T_{mean} is the daily mean temperature.

Furthermore, the weighted daily precipitation (Rw) was determined using the formula proposed by Taylor et al. (2012). This predictor acknowledges that soil can only dry out progressively following a rainfall event. Therefore, the use of Rw allows for the consideration of the latent effect of precipitation on soil water status.

$$Rw_t = \alpha \times R_t + (1 - \alpha) \times Rw_{t-1} \tag{3}$$

where R_t is the measured daily precipitation at day t, Rw_{t-1} is the weighted precipitation value for the previous day t-1, α is a weighting

Table 1
Summary of predictors used for modeling.

Source data	Predictors	Unit	Code
iG-Apex	iG-Apex	no unit	a
	Inflection point	day	x0
	Slope at the inflection point	day^{-1}	k
	Variation of iG-Apex between two observations	no unit	da
	Days between two observations	day	diff_day
-	Last observed Ψpd	MPa	pm1
Temperature	Growing degree day	°C. day	GDD
	Cumulative growing degree day	°C. day	cGDD
	Minimum daily temperature	°C	Tmin
	Maximum daily temperature	°C	Tmax
	Minimum daily temperature in the previous 3 days	°C	Tmin3
	Maximum daily temperature in the previous 3 days	°C	Tmax3
	Minimum daily temperature in the previous 7 days	°C	Tmin7
	Maximum daily temperature in the previous 7 days	°C	Tmax7
	Accumulated GDD between 2 dates of apex observation	°C. day	GDD_cumul
Relative humidity	Relative humidity of the day	%	RH
	Minimum RH in the previous 3 days	%	RHmin3
	Maximum RH in the previous 3 days	%	RHmax3
	Minimum RH in the previous 7 days	%	RHmin7
	Maximum RH in the previous 7 days	%	RHmax7
	Accumulated RH between 2 dates of apex observation	%	RH_cumul
Precipitation	Weighted daily precipitation	mm	Rw
	Minimum Rw in the previous 3 days	mm	Rwmin3
	Maximum Rw in the previous 3 days	mm	Rwmax3
	Minimum Rw in the previous 7 days	mm	Rwmin7
	Maximum Rw in the previous 7 days	mm	Rwmax7
	Accumulated Rw between 2 dates of apex observation	mm	Rw_cumul
Potential evapo-transpiration	Daily potential evapotranspiration	mm	ET0
	Accumulated ET0 between 2 dates of apex observation	mm	ET0_cumul
Precipitation, ET0	Daily climate water balance	mm	WS

factor and was set to 0.3.

In parallel, in order to quantify the degree of soil drying process, daily climate water balance (*WS*) was computed.

$$WS = R - ET0 \qquad (4)$$

where R is daily rainfall, and ET0 is daily potential evapotranspiration.

In order to account for weather variables' correlation with vine water status in a previous short period, minimum and maximum observed values of certain weather variables in the previous 3 or 7 days were also used as predictors, noted as respectively: *Tmin3, Tmax3, Tmin7, Tmax7, RHmin3, RHmax3, RHmin7, RHmax7, Rwmin3, Rwmax3, Rwmin7,* and *Rwmax7*.

In order to account for the variation between two Ψpd observations (details will be given in Section 2.4.3.2), the accumulation of certain weather variables between two dates of Ψpd measurements were also calculated, and used as predictors (*GDD_cumul, RH_cumul, ET0_cumul,* and *Rw_cumul)*. These predictors were not calculated for the first observation of each time series.

$$Variable_{cumul} = \sum_{date\ of\ previous\ \Psi pd\ observation}^{date\ of\ current\ \Psi pd\ observation} daily\ variable\ value \qquad (5)$$

Given that Ψpd tends to show a global decreasing trend in time (Lebon et al., 2003), temporal information might be able to explain Ψpd evolution. Therefore, the Cumulative Growing Degree Day (*cGDD*) was derived by summing GDD from April 1st to September 30th, and

calculated at a daily time step.

2.3.3. Datasets for modeling

Predictors presented in Table 1 were associated to all available measured Ψpd. Measurements which did not have the full set of predictors (n=30) were omitted. The final dataset contained 516 lines, derived by merging the datasets from the two experimental sites. In the final dataset, Ψpd measurements spanned from −1.4–0 MPa, while observed iG-Apex ranged from 0 to 1. However, the majority of Ψpd measurements (about 95 %) were beyond −0.8 MPa.

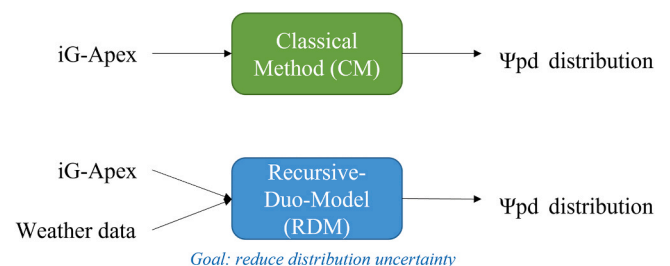*2.4. Ψpd models*

2.4.1. General approach

Two methods for modeling Ψpd were compared (Fig. 2). Their main specificities are highlighted here, while detailed explanations will follow in the next sections. The first method, named the Classical Method (CM) only depends on iG-Apex observations. It was inspired by the method proposed by Pichon et al. (2023), and was considered, in this work, as a reference approach. The second method, named the Recursive-Duo-Model (RDM), utilized both iG-Apex observations and weather data to perform Ψpd predictions. In order to account for uncertainty, both CM and RDM generated distributions of possible Ψpd values, instead of a single value (McElreath, 2016). By considering both iG-Apex and weather data, and by modeling Ψpd's auto-correlation, RDM aimed at reducing estimation uncertainty.

2.4.2. Classical method (CM)

Following Pichon et al. (2023), ten iG-Apex intervals were associated to ten average Ψpd values (Fig. 3). The uncertainty of each value was characterized by observed standard deviation of Ψpd within each interval. Based on this work, the objective of the Classical Method (CM) was to obtain a realistic Ψpd distribution for each iG-Apex observed at date t (a_t).

A Look Up Table (LUT) was built using data from Pichon et al. (2023) (Fig. 3). It contained means (μ_p) and standard deviations (σ_p) of Ψpd observations for ten intervals of iG-Apex (0–0.1, 0.1–0.2, …, 0.9–1). Using this LUT, each a_t could be associated to an iG-Apex class, thereby to a pair of mean and standard deviation. It was assumed that in each iG-Apex class, observed Ψpd follow a Normal distribution truncated at zero, as positive Ψpd are physically uninterpretable. For each a_t, 1 000 possible Ψpd values were simulated using μ_p and σ_p to construct a distribution at date t (noted as P_t), with positive samples' values reduced to 0.

All data in the study of Pichon et al. (2023) were used to construct the LUT. The goal was to compare CM-generated predictions, that were based on all available historical data, with predictions given by the proposed Machine-Learning-based method, which was presented in the next section.

Fig. 2. A conceptual diagram of the two methods for Ψpd modeling compared in this paper.
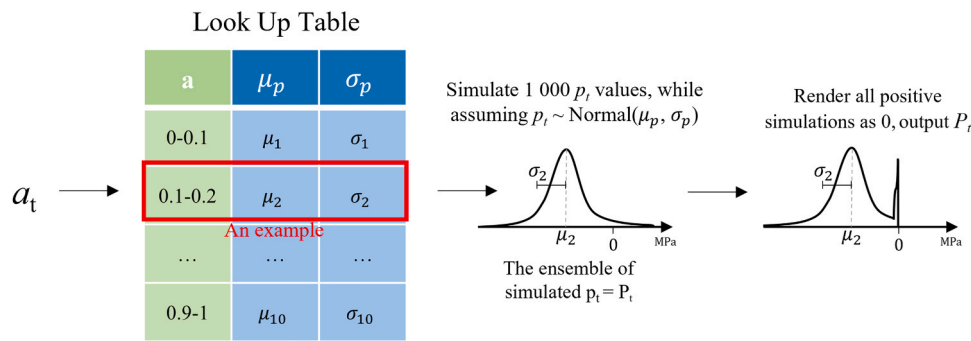
Look Up Table

Fig. 3. A graphical illustration of the Classical Method for predicting Ψpd.

2.4.3. Recursive–duo-model method (RDM)

2.4.3.1. General idea. The main goal of the RDM was to reduce prediction uncertainty stemmed from the CM. Hence, the RDM was only activated when CM-generated distributions are considerably uncertain (evaluation criterion will be presented in Section 2.5.2). In order to reduce uncertainty, the RDM included three functions: 1) generating a pseudo-observation of Ψpd using two models, 2) modifying a CM-generated distribution with the pseudo-observation through resampling, and 3) collecting historical predictions.

2.4.3.2. Generation of the pseudo-observation of Ψpd. The pseudo-observation was obtained by merging two predicted Ψpd derived from two different Random Forest (RF) models (Liaw and Wiener, 2002), giving rise to the term "Duo" in the method's name. The choice of the RF algorithm was for its simple implementation and it has been proved to be robust and able to handle high-dimensional modeling scenario.

The first RF model was trained to directly predict Ψpd at date *t*, thereby called "direct model". It played a classical role in the RDM like in other regression problems, consisting of generating a large number of decision trees and output the final prediction by aggregating predictions given by each tree. This RF model gave the first Ψpd prediction. The direct model was trained using a set of predictors containing 21 predictors: *a, GDD, cGDD, Tmin, Tmax, RH, Rw, ET0, WS, Tmin3, Tmax3, Tmin7, Tmax7, RHmin3, RHmax3, RHmin7, RHmax7, Rwmin3, Rwmax3, Rwmin7, Rwmax7* (Table 1).

The second RF model aimed at modeling Ψpd's temporal autocorrelation. Instead of directly predicting Ψpd at date t (like the direct model), the second model predicted the *variation* of Ψpd between two measurement dates. A Ψpd prediction at date t was obtained by accumulating a certain number of predicted Ψpd variations based on a previously predicted Ψpd. The number of variations was set to be 2 in this study. Hence, the second RF model is referred to as the cumulative model. The cumulative model was trained using another set of predictors containing 9 predictors: *pm1, da, diff_day, x0, k, GDD_cumul, RH_cumul, ET0_cumul, Rw_cumul* (Table 1). The predictor *pm1* stands for previous Ψpd measurements, which was proposed by Pòças et al. (2020) for considering the temporal dynamic of Ψpd. Observed previous Ψpd measurements were used as *pm1* for model training.

The pseudo-observation was computed as the average of the two predictions, noted as $p^{pseudo\ obs}_t$. This value was then used in resampling.

For training both direct and cumulative models, the *randomForest()* function was utilized with the following parameter settings: the number of trees was set to 500, and the number of variables randomly sampled was set to 7 for the direct model and 3 for the cumulative model.

In order to obtain the optimum data proportion for training the RDM, learning curves for both the training and testing phases were generated by varying the percentage of time series included in the training set. The examined percentages were 40 %, 45 %, 50 %, 55 %, up to 90 %. For each percentage, training and testing sets were randomly created 100 times. Root Mean Square Error (RMSE) was used as the performance metric (Kuhn and Johnson, 2013). The results are shown in Appendix A. After analysing the learning curves and considering practical implications related to the training set size, 70 % of the dataset (52 time series) were chosen for the RDM training.

2.4.3.3. Resampling. The resampling method was adapted from the Particle Filter algorithm presented by Arulampalam et al. (2002) and Montzka et al. (2011). It was used to modify a CM-generated distribution considered too dispersive, by using the pseudo-observation. For the record, a CM distribution is represented by 1 000 possible values of Ψpd. These values are referred to as "samples". The goal of resampling was to reduce the diversity of these samples (Fig. 4). This was realized through three steps: firstly, initialize an equivalent probability for all samples; secondly, assess the numerical discrepancy between each sample and the pseudo-observation, and attribute a new probability to each sample given that discrepancy information; and thirdly, generate 1 000 samples from the initial set based on the new probabilities (details of the algorithm were given in Appendix B). This procedure allowed that samples exhibiting larger discrepancies towards the pseudo-observation are less likely to be selected in the third step, thereby reducing the diversity of the initial set of samples. The resulting new set of samples was output as the RDM-generated Ψpd distribution at current date t (still noted as P_t).

2.4.3.4. Collection of historical predictions. After resampling, the median of a RDM-generated distribution was memorized as a historical prediction of Ψpd. The same operation was realized for CM-generated distributions. Historical predictions were crucial for the functioning of the cumulative model. On the one hand, the cumulative must accumulate predicted Ψpd variations on a historical value. On the other hand, since the predictor *pm1* (last observed Ψpd, required by the cumulative model) should not be available in practice, historical predictions were thus used as *pm1*. This mechanism enabled previous Ψpd predictions to directly impact the current prediction at date *t*, while the latter could further impact predictions in future, giving rise to the term "Recursive" in the method's name. This process was repeated until the last Ψpd value in the time series had been predicted. The overall workflow in the RDM is summarized in Fig. 5.

2.5. Evaluation

2.5.1. Scenarios of evaluation

Performances of the CM and RDM were evaluated in four scenarios corresponding to different levels of water deficit. Each scenario was defined according to a water deficit class for grapevines, as proposed by Deloire et al. (2020). The first scenario corresponded to no water deficit (-0.3 ≤ observed Ψpd < 0 MPa), the second one corresponded to mild to moderate water deficit (-0.5 ≤ observed Ψpd < −0.3 MPa), the third one corresponded to moderate to severe water deficit (-0.8 ≤ observed Ψpd < −0.5 MPa), and the last scenario corresponded to severe to high water
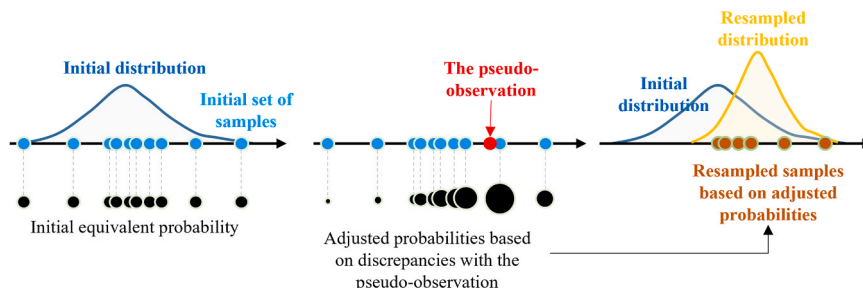
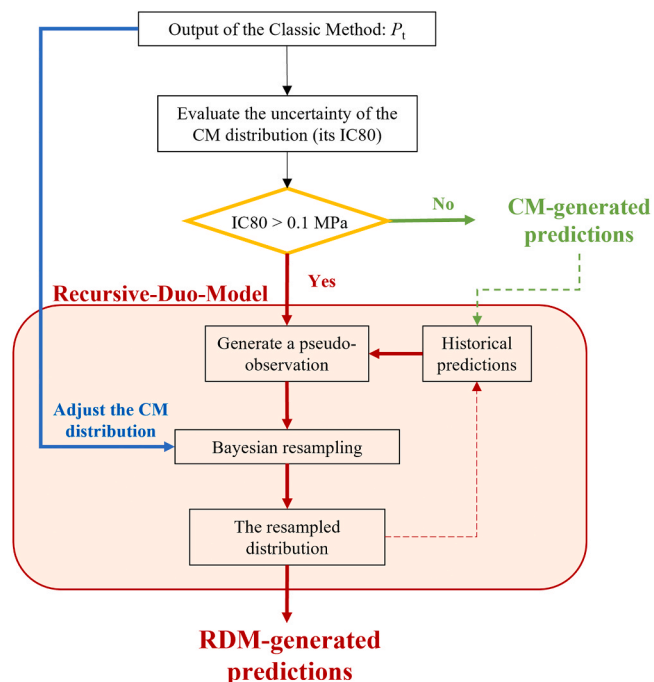**Fig. 4.** A graphical illustration of the Bayesian resampling mechanism.

Fig. 5. A graphical illustration of the Recursive-Duo-Model method for predicting Ψpd. "IC80" stands for the 80 % interval of confidence.

deficit (presence of water stress) (observed Ψpd < −0.8 MPa).

In the training dataset, these four scenarios contained respectively 258, 131, 101, and 26 lines of data (containing Ψpd and predictors).

2.5.2. Prediction performance scores

Accuracy of predictions of CM and RDM approaches was assessed by Mean Absolute Error of Median (MAEM). MAEM was calculated by measuring absolute errors between medians of predicted distributions and actual observations of Ψpd. The lower was this value, the better was a method in predicting water deficit.

Uncertainty of predictions of CM and RDM was evaluated by 80 % Interval of Confidence (noted IC80). It was estimated by calculating the difference between the limits of 90 % and 10 % percentiles of a predicted distribution. Therefore, IC80 corresponded to the width of the interval that covers 80 % of the most probable prediction values. IC80 was also used to evaluate the level of uncertainty of a predicted distribution, which permits running the RDM. If IC80 ≤ 0.1 MPa, the uncertainty of predicted distribution was considered acceptably low (Section 2.4.3).

2.5.3. Cross-validation and statistical test

The full dataset contained 82 time series of Ψpd, each consisting of at least three observations. According to Appendix A, 70 % of time series were randomly selected from the original dataset for model training,

while the remaining 25 time series (30 % of the dataset) were used for testing. Ψpd values were predicted using the CM and RDM approach, and these predictions were compared with observed values in the testing dataset using R^2 and RMSE. The two performance scores, MAEM and IC80 (see Section 2.5.2), were calculated based on this comparison. A Cross-Validation (CV) procedure was conducted by randomly generating the training set 100 times, resulting in 100 MAEM and IC80 values. The t-test was used to detect significant differences between the performance scores produced by the two methods during CV in each of the four water deficit scenarios.

2.6. Software

All sample generations and statistical analyses were performed using R (R Core Team, 2021). For modeling the logistic regression of iG-Apex (Section 2.3.1), the sum of squared ε in the logistic regression was minimized by adjusting values of x0 and k, using the R function *optim()* (with initial condition: [x0= 180; k= 0.5]).

3. Results

Focusing on predictions obtained from one of the 100 testing datasets, observed Ψpd varied between −1.1 and −0.05 MPa (Fig. 6). Ψpd predicted by the CM varied between −0.6 and −0.1 MPa (Fig. 6a), while those predicted by the RDM varied between −1 and −0.1 MPa (Fig. 6b). CM predictions were around the reference line for observed Ψpd ranging from −0.5 and −0.1 MPa, but far from it for observed Ψpd between −1 and −0.5 MPa (Fig. 6a). The predictions given by the CM seemed to saturate above −0.5 MPa with no prediction lower than −0.6 MPa and many predictions close to −0.58 MPa. Conversely, RDM predictions were closer to observed Ψpd (R^2 = 0.608 vs 0.58), and showed a better global coherence with observations (RMSE = 0.139 vs 0.144) than CM predictions. For strong water constraint (observed Ψpd between −1 and −0.5 MPa), RDM predictions were closer to the reference line than CM predictions. Notably, very negative Ψpd were predicted by RDM (down to −0.9 MPa) (Fig. 6b), which were missing among CM predictions.

In terms of prediction uncertainty, the average 80 % Interval of Confidence (IC80) generated by the CM was 0.363 MPa, while that of the RDM was 0.202 MPa: globally, prediction intervals of RDM were much narrower. The uncertainty also varied according to observed values of Ψpd. For CM, IC80 increased drastically when predicted values decreased, raising from about 0.2 MPa to more than 0.6 MPa in width. When observed water deficit was high, CM distributions extended from about −0.25 MPa to −0.9 MPa (Fig. 6a). While for the RDM, wide prediction intervals still appeared for lower predicted values, but were much less frequent than the CM. Indeed, under high water deficit, RDM's IC80 was around 0.3 or 0.4 MPa, and was seldom greater than 0.6 MPa. Consequently, the upper bounds of RDM distributions were generally below −0.4 MPa (Fig. 6b).

Focusing on all 100 testing datasets, 15 600 predicted distributions Ψpd (for both CM and RDM) were obtained, providing more generalized descriptions on method performance. The Mean Absolute Error of
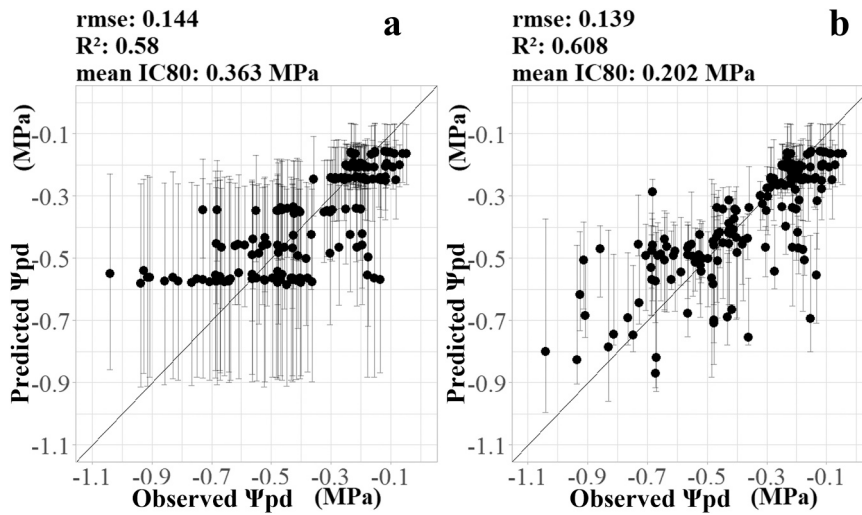
Fig. 6. Observed Ψpd in a representative testing dataset and their predictions with prediction intervals generated by (a) Classical Method, and (b) Recursive-Duo-Model Method. Points, upper bounds, and lower bounds represent respectively, medians, 90 % percentiles, and 10 % percentiles of predicted distributions.

Median (MAEM) was generally low for the first three water deficit scenarios (Fig. 7), while showed significant degradation in the fourth scenario. No significant difference in MAEM (p = 0.2) was observed between CM and RDM when there was no water deficit (Fig. 7a – scenario 1). When there was mild to moderate water deficit (scenario 2), the RDM produced slightly smaller MAEM than the CM, with a significant reduction of 0.01 MPa (p < 0.001) (Fig. 7b). When water deficit is moderate to severe (scenario 3), RDM method did not significantly improve MAEM compared to CM (p = 0.31) (Fig. 7c). When water deficit was high and stress was present (the fourth water deficit scenario), RDM reduced significantly MAEM by −0.1 MPa compared to CM (p < 0.001) (Fig. 7d).

In addition to prediction accuracy, uncertainty of predicted Ψpd was equally compared (Fig. 8). The RDM brought net reductions of 80 %

Interval of Confidence (IC80) in all four water deficit scenarios. When predicting the first water deficit scenario (no deficit), the RDM reduced significantly IC80 by 0.07 MPa compared to the CM (p < 0.001) (Fig. 8a). When predicting the second water deficit scenario (mild to moderate deficit), the RDM method reduced significantly IC80 by 0.21 MPa in comparison with the CM (p < 0.001) (Fig. 8b). For moderate to severe water deficit (scenario 3), the RDM reduced IC80 significantly by 0.27 MPa (p < 0.001) compared to the CM (Fig. 8c). With high water deficit (water stress), RDM's IC80 was always significantly smaller than the CM, by 0.29 MPa (p < 0.001). In this case, average IC80 of RDM was still high (0.33 MPa) but significantly reduced when compared to that of CM which was up to 0.62 MPa (Fig. 8d – scenario 4).

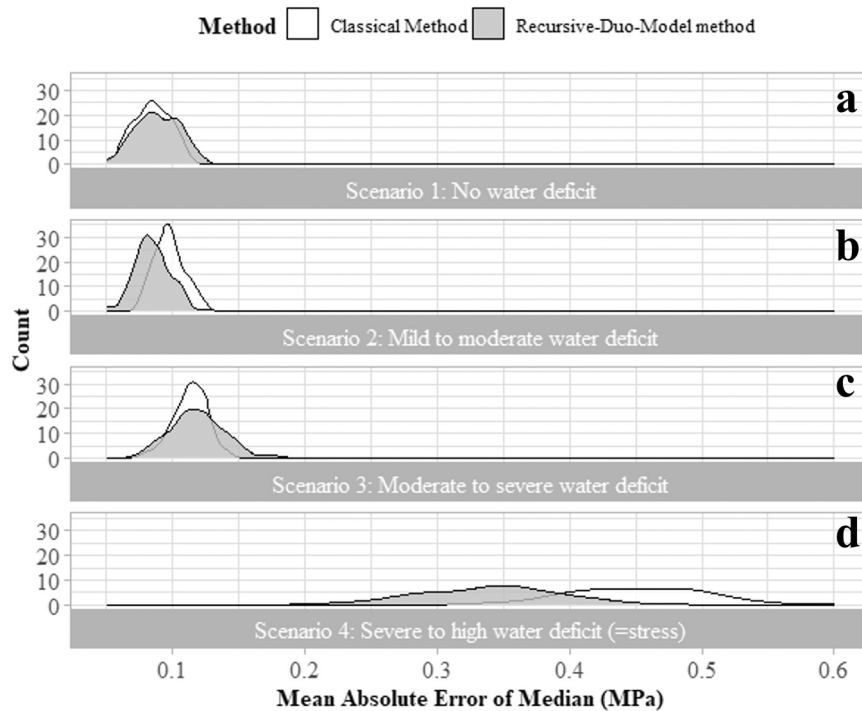In order to fully compare water deficit classifications made by both

Fig. 7. Distributions of Mean Absolute Error of Median (MAEM) of Ψpd predictions according to four water deficit scenarios (a-d) when accounting for all 100 randomly generated testing datasets.
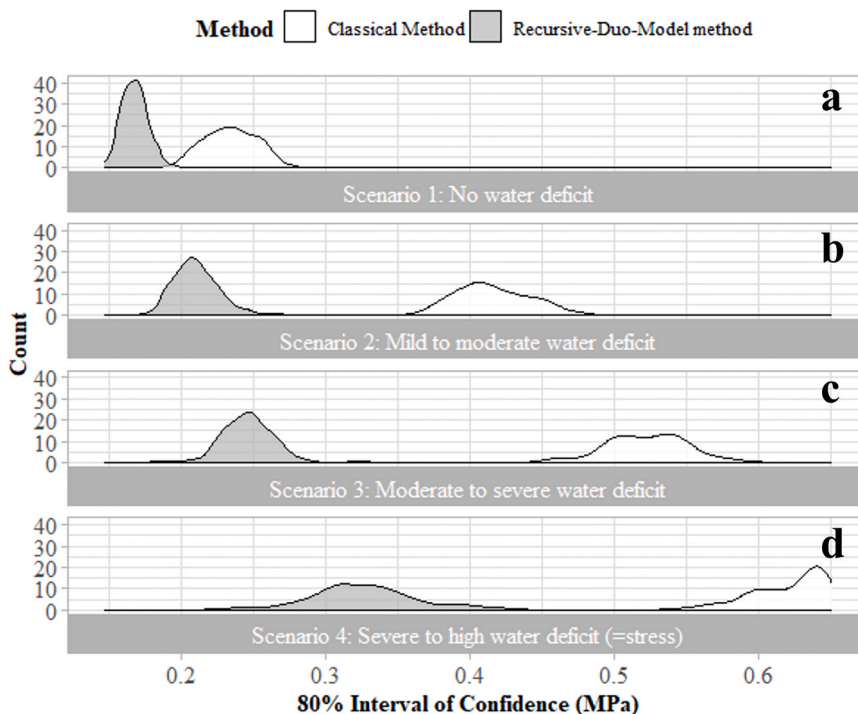
Fig. 8. Distributions of 80 % Interval of Confidence (IC80) of Ψpd predictions according to the four water deficit scenarios (a-d) when accounting for all 100 randomly generated testing datasets.

methods, two confusion matrices were built (Fig. 9). Both methods were strong in detecting the absence of water deficit, given that more than 70 % of CM and RDM predictions predicted the correct class when no water deficit was observed. Regarding the mild to moderate water deficit scenario (observed class=2), in average, the RDM produced 54.21 % predictions in the correct class, while CM produced only 39.14 %. Moreover, the CM tended to predict the class-2 water deficit as "no water deficit", while wrongly placing 29.32 % of predictions in latter class (Fig. 9a). In the case of moderate to severe water deficit (observed class=3), 53.72 % of RDM predictions were correct, with 35.34 % of predictions in class 2 and very few (about 5 %) of predictions

were in class 1. In contrast, only 38.72 % of CM predictions were in class 3, close to the percentage observed in class 2 (34.72 %), and there was up to 16 % of CM predictions which were still in class 1 (Fig. 9a). Lastly, when predicting severe to high water deficit (observation=class 4), both methods placed the majority of their predictions in class 3 instead of class 4, while less than 20 % of predictions were located in the correct class. However, the RDM generated more predictions in class 4 and 3 (18.36 + 60.29 = 78.65 %) than the CM (42.01 + 16.57 = 58.59 %), showing more coherence in predicting higher water deficit (Fig. 9b).
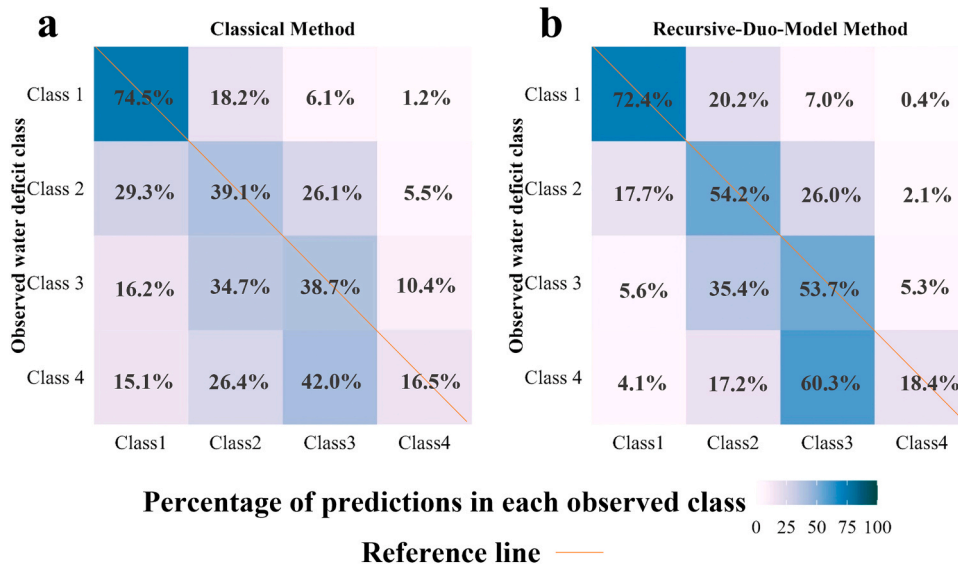

Fig. 9. The confusion matrices showing the four observed water deficit classes and mean percentage of predictions in each class produced by (a) Classical Method (CM) and (b) Recursive-Duo-Model Method (RDM). Numbers in matrix cells correspond to the mean percentages calculated from all predictions in 100 testing datasets.

4. Discussion

4.1. The improvement of prediction accuracy: comparison and interpretation

The Recursive-Duo-Model (RDM) was introduced for estimating Predawn Leaf Water Potential (Ψpd), by using time series of vine shoot growth observations (iG-Apex), weather data, and a mechanism accounting for prior Ψpd information. This approach was compared with the Classical Method (CM) that relies solely on vine shoot observations. This comparison revealed several noteworthy improvements achieved by the RDM.

For the second and third water deficit scenario (Ψpd from −0.8 to −0.3 MPa), both CM and RDM achieved a low level of error, with Mean Absolute Error of Median (MAEM) globally ranging from 0.05 to 0.15 MPa (Fig. 7b-c). This could be explained by the strong correlation between iG-Apex and Ψpd when the latter varies between −0.8 and −0.2 MPa (Pichon et al., 2023).

However, Fig. 6 showed that the RDM had better RMSE and R^2 than the CM, while aligning closely with metrics from certain Ψpd predictive models based on multi/hyper-spectral data in some previous studies (Giovenzana et al., 2018; Pôças et al., 2020). Several factors could have contributed to the prediction accuracy of the RDM: i) the utilization of multiple sources of information, iG-Apex and weather data, as recommended by Diago et al. (2022), was found to be relevant in assessing vine water status; ii) the incorporation of Ψpd temporal dynamic in the modeling process, following the practice suggested by Pôças et al. (2020), could have also improved the performance.

Concerning the class with the strongest water deficit (for Ψpd < −0.8 MPa), where iG-Apex becomes uninformative due to stopped vine shoot growth, the RDM exhibited the MAEM level around 0.35 MPa. This limitation arises from the uninformative iG-Apex/Ψpd relationship when iG-Apex approaches to zero (Pichon et al., 2023). The low amount of training data belonging to this deficit scenario could be an important factor responsible to the poor performance of the model. Indeed, such observations were not frequent, because high water deficit might only be observed on soils with a weak water holding capacity, and when a dry period lasted for a long duration, which was a rare situation in the studied area.

Nevertheless, the RDM outperformed the CM, as evidenced by a significant reduction in MAEM in cross-validation results (Fig. 7d). This positive impact can be attributed to the cumulative model in the RDM, which is stronger in obtaining lower Ψpd values. The inclusion of weather data might further contribute to model low-value Ψpd.

Regarding the scenario without water deficit (Ψpd > −0.3 MPa), the similarity in predictions between the CM and RDM (Fig. 7a) can be explained by the RDM's activation mechanism. Indeed, the RDM was only triggered when a CM-generated Ψpd distribution is considerably uncertain, which was not prevalent in the majority of cases in the first water deficit scenario (Pichon et al., 2023).

In general, the RDM well predicted Ψpd between −0.8 MPa to 0 MPa, a range comparable to many Ψpd predictive models reviewed by Tosin et al. (2022). However, such prediction accuracy is inferior to spectral-data-based models reported in the studies of Tosin et al. (2021) and Tosin et al. (2022), where distinct data sources, predictors, and learning algorithms were employed, alongside differences in Ψpd measurement protocol. Besides, the RDM provides uncertainty information (Section 4.2), and has certain important operational advantages in data collection over spectral-based models (Section 4.3). Moreover, the RDM proposed a modeling structure that combines machine learning and Bayesian resampling, which could be adapted to model other temporally auto-correlated variables.

4.2. Prediction uncertainty: quantification and reduction

The uncertainty of CM and RDM predictions was evaluated by 80 % Interval of Confidence (noted IC80). Such uncertainty stems from various factors in field, like plant variety, soil type, weather conditions, and/or the transpiration capacity of vines (García-Tejera et al., 2021). The uncertainty information also indicated an upward trend for both methods as water deficit increased (Fig. 8). The increasing uncertainty in CM predictions aligned with the observed relationship between Ψpd and iG-Apex. Over time, Ψpd is continually influenced by various field factors, as mentioned earlier, while iG-Apex tends to approach 0. Progressively, similar iG-Apex values could be associated with significantly different Ψpd values. Relied on CM-generated distributions, the RDM-generated ones were equally impacted by this mechanism.

When comparing IC80 results derived from the CM and RDM, the reduction of IC80 achieved through resampling was evident across all water deficit scenarios (on average, a reduction of 0.07–0.29 MPa in IC80). The result for the scenario with no water deficit might be surprising, because readers may wonder that the RDM might not be activated in that scenario. Yet, high Ψpd values (between −0.3 and 0 MPa) could be observed when iG-Apex was low because of rainfall, thereby allowing the activation of the RDM. Otherwise, the RDM well reshaped CM-generated distributions, notably for the second and third water deficit scenarios, where RDM-generated distributions were much less dispersive (Fig. 9). These results highlighted the relevance of the resampling algorithm, as the observed uncertainty reduction ran in parallel with the maintenance and even improvement of Ψpd prediction accuracy. This could be attributed not only to the incorporation of weather data in predictive models, but also to the mechanism of accounting for temporal auto-correlation of Ψpd, which both allowed the generation of relevant pseudo-observations.

4.3. Operational implications of the RDM

The RDM demonstrated a strong ability to detect the first three water deficit scenarios with high certainty (Fig. 9b). Operationalizing the RDM in this context could hold significance, especially for situations where proactive practices are crucial. In Mediterranean vineyards, soil and canopy managements are most effective before berries begin to ripen (Keller, 2005), in other words, when vines can still draw water from the soil and use that water to aliment berries. These operations should be done before the presence of a significant water stress.

Therefore, as suggested by Pichon et al. (2023), vinegrowers can make regular iG-Apex in the beginning of summer (e.g. after flowering and before véraison), while the RDM allows to transform these observations into Ψpd predictions with a higher level of confidence. Predicted Ψpd could be used to fine-tune vine water status of a given parcel according to its production objective (Leeuwen et al., 2009). Under specific conditions, these predictions could also be used to launch urgent irrigation.

In terms of data requirement, the RDM relies on two easily accessible data sources: vine shoot observations and weather data. Although the RDM requires more than twenty weather-related predictors, only four types of weather information are actually required (temperature, relative humidity, precipitation, and potential evapo-transpiration), which are easy to obtain. In contrast to spectral-based models commonly reported in the literature, iG-Apex measurements can be acquired whenever in the day using a smartphone (Brunel et al., 2019), without specific weather or light conditions, or the need for handheld/airborne spectrometers (Pôças et al., 2015). In parallel, while the RDM models Ψpd temporal dynamic, it doesn't necessitate actual previously observed water potential readings like what was suggested by Pôças et al. (2020) and Tosin et al. (2021), reducing further operational constraints.

The RDM requires time series of iG-Apex longer than two observations (collected from approximatively three weeks) to be fully operational. Such practice of regular field visiting should not impose a substantial addition to vinegrowers' weekly responsibilities (Acevedo-Opazo et al., 2010b). In some wine regions in Southern France, monitoring Ψpd has been part of professionals' routine, and such

measurement could be required at a large number of locations (Baralon et al., 2012). The proposed model could reduce significantly their operational charges and facilitate spatial vine water status monitoring. Nevertheless, the collection of iG-Apex could be interrupted by canopy operations like shoot trimming (Pellegrino et al., 2005; Pichon et al., 2023). Therefore, it is recommended to place the iG-Apex measurement before shoot thinning, or at least a week after each operation.

The uncertainty information provided by the RDM could be an indicator of the reliability of model predictions (Linde et al., 2017). For instance, in scenarios with no water deficit (the first scenario), both the CM and RDM yield small prediction errors and low IC80, signifying "reliable" predictions for decision-making. Conversely, in the scenario with high water deficit, generally high IC80 values signal to users the need for careful consideration when using those predictions, and perhaps the integration of actual Ψpd measurements, and/or additional vine water status data (e.g. sap flow measurements, stem water potential) (Tuccio et al., 2019) to confirm the presence of water stress. In cases where vinegrowers derive actual Ψpd observations, these observed values could be integrated into the RDM (to be coupled with the cumulative model), in order to improve the prediction accuracy for future vine water status. Moreover, uncertainty information itself may convey critical messages to vinegrowers, a perspective seldom explored by modelers. As shown in Fig. 8, a high IC80 of a predicted Ψpd should serve as an alarming sign to vinegrowers about the potentially severe water deficit in their vines; vice versa. Although not quantitative, this message might still be a valuable input for decision-making.

4.4. Limitations of the study and future improvements

While the prediction uncertainty of the RDM has been reduced, the method showed poor performance in detecting high water deficit (the fourth deficit class, Ψpd < −0.8 MPa). A key factor limiting the RDM's accuracy in this scenario was the training data. A notable issue was the imbalance in the training dataset, where only 5 % of Ψpd observations were lower than −0.8 MPa. This imbalance presents a challenge for conventional classifier algorithms, as discussed by Sun et al. (2007). Adopting cost-sensitive algorithms (Benkendorf et al., 2023) could improve prediction performance.

In parallel, as pointed out by García-Tejera et al. (2021), water potential is not just an indicator of soil water depletion, but the result of interactions between plant roots and various environmental factors, notably soil. No soil information was used in the RDM. To tackle down this issue, as shown by Roux et al. (2019), the Total Transpirable Soil Water (TTSW) is an important driver of Ψpd variation: the lower the TTSW, the more sensitive Ψpd is to weather conditions. Hence, it might be interesting to incorporate open-access soil data, like TTSW estimation (Román Dobarco et al., 2019), into the RDM.

The generation of pseudo-observations could be improved. In this study, the pseudo-observation was considered as a single value, while it could be considered as a distribution. Instead of using Random Forest algorithm for model training, Quantile Regression Forest (Meinshausen, 2006) could be applied to generate the pseudo-observation. Moreover, preliminary results (not shown) have indicated that the direct model generally performs better at the beginning of summer, or under low water deficit conditions. Conversely, the cumulative model may be more informative when there is high water deficit. Therefore, it might be relevant to assign varying weights to the direct and cumulative models based on specific criteria (e.g. cumulative GDD, observed iG-Apex).

Pichon et al. (2023) demonstrated that the relationship between iG-Apex and Ψpd can be sensitive to vine cultivar. In this study, two red cultivars, cv. Grenache and cv. Syrah, were selected because they are both widely grown under Mediterranean climate and they display similar phenology and leaf growth responses to soil water deficit (Lebon et al., 2006; Destrac-Irvine and Van Leeuwen, 2018). This suggests that practitioners may need to recalibrate the model for cultivars that differ significantly from those studied, in terms of vegetative growth under

water deficit. However, the objective of this paper is not to propose a universally applicable model for diverse vine cultivars, but rather to demonstrate the utility of iG-Apex and the proposed modeling structure.

In its current form, the RDM model has been developed using data exclusively collected from rainfed vineyards, limiting its applicability to similar cultural systems. Although dry farming systems are common in the Mediterranean wine-making region, facing climate change, research efforts could focus on adjusting and retraining the RDM using data gathered from irrigated vineyards. This would allow for the consideration of the impact of irrigation on Ψpd modeling.

5. Conclusion

The Recursive-Duo-Model (RDM) offers a novel approach for predicting predawn leaf water potential (Ψpd). By deploying time series of two easily accessible information: vine shoot growth and weather data, the RDM showed particular strengths in accurately predicting Ψpd for absent to severe water deficit scenarios (-0.8≤ observed Ψpd≤ 0 MPa). It proposed a mechanism that accounts for prior vine water status in current predictions, hence improved Ψpd predictions when there is high water deficit (observed Ψpd ≤ −0.8 MPa). By combining machine learning and Bayesian resampling, the RDM quantified and reduced significantly prediction uncertainty compared to an approach which depends uniquely on vine shoot growth data. Practically, the RDM encourages practitioners to make regular iG-Apex measurements at the beginning of summer, and to evaluate the predicted Ψpd by considering the associated prediction uncertainty. This latter helps practitioners to identify periods where iG-Apex and weather data could not accurately predict Ψpd, while optimizing the timing for acquiring reference vine water status data. However, further advancements are needed to improve the RDM, especially on its ability to accurately detect high water deficit. Soil and/or other ancillary information should be incorporated into the predictive model to further improve prediction accuracy. A more balanced training dataset should also improve the model's performance in detecting the presence of high water deficit.

CRediT authorship contribution statement

Yulin ZHANG: Writing – original draft, Methodology, Investigation, Formal analysis. **Léo Pichon:** Writing – review & editing, Methodology, Conceptualization. **Anne Pellegrino:** Validation, Resources. **Sébastien Roux:** Validation, Resources. **Cécile Péruzzaro:** Investigation. **Bruno Tisseyre:** Writing – review & editing, Supervision, Conceptualization.

Declaration of Competing Interest

The authors declare the following financial interests/personal relationships which may be considered as potential competing interests: Yulin Zhang reports financial support was provided by **Digitag ANR-16-CONV-0004**. Yulin Zhang reports financial support was provided by Région Occitanie.

Data availability

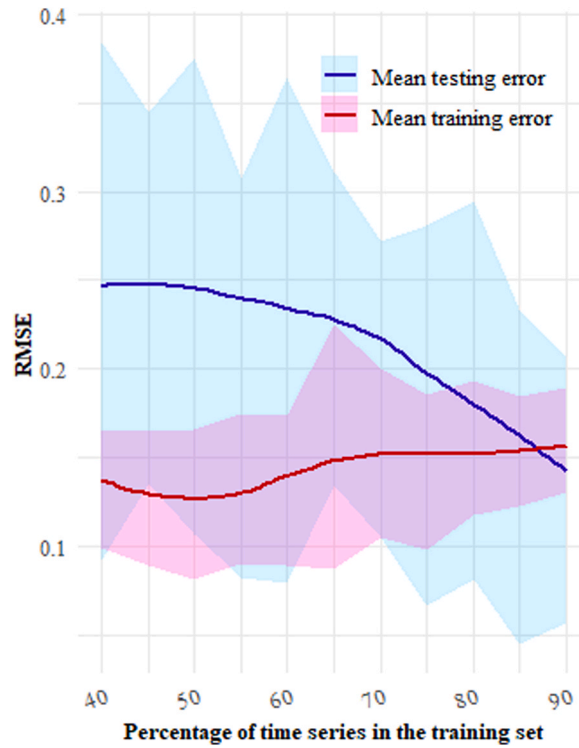Data will be made available on request.

Appendix A. Learning curves of the Recursive-Duo-Model (Mean, 25th and 75th percentiles of Root Mean Square Error (RMSE))

Appendix B. Algorithm: An adapted Bayesian resampling algorithm

(continued)

Input:
- N: Total number of samples (set to 1 000)
- Prior: Vector of samples generated by the Classical Method (size N)
- $\mathbf{p}^{pseudo\ obs}_t$: Pseudo-observation generated by the direct and cumulative model (size 1)

Output:
- $\mathbf{P_t}$: Vector of output samples (size N)

Procedure:
1. Initialize sample weights:
   For each sample in Prior i from 1 to N:
      Initialize initial weight $\mathbf{w_i}$ to 1/N

2. Calculate discrepancy and adjust sample weights:
   For each sample in Prior i from 1 to N:
      Calculate discrepancy $\mathbf{d_i}$ as the absolute difference between the sample and $\mathbf{p}^{pseudo\ obs}_t$, raised to the power of 0.75
      Add a small constant ($1*10^{-7}$) to $\mathbf{d_i}$ to avoid division by zero
      Calculate adjusted weight $\mathbf{wa_i}$ as $\mathbf{w_i}$ / $\mathbf{d_i}$

   Normalize $\mathbf{wa}$ by dividing each weight by the sum of all weights in $\mathbf{wa}$

3. Resample samples in Prior based on adjusted weights:
   Initialize an empty vector $\mathbf{P_t}$
   Repeat N times:
      Randomly select a member index based on the probabilities in $\mathbf{wa}$
      Add the corresponding sample in Prior to $\mathbf{P_t}$

End Procedure

References

Acevedo-Opazo, C., Tisseyre, B., Ojeda, H., Guillaume, S., 2010a. Spatial extrapolation of the vine (Vitis vinifera L.) water status: a first step towards a spatial prediction model. Irrig. Sci. 28, 143–155. https://doi.org/10.1007/s00271-009-0170-3.

Acevedo-Opazo, C., Tisseyre, B., Taylor, J.A., Ojeda, H., Guillaume, S., 2010b. A model for the spatial prediction of water status in vines (Vitis vinifera L.) using high resolution ancillary information. Precis. Agric. 11, 358–378. https://doi.org/10.1007/s11119-010-9164-7.

Albrizio, R., Puig-Sirera, À., Sellami, M.H., Guida, G., Basile, A., Bonfante, A., Gambuti, A., Giorio, P., 2023. Water stress, yield, and grape quality in a hilly rainfed "Aglianico" vineyard grown in two different soils along a slope. Agric. Water Manag. 279, 108183 https://doi.org/10.1016/j.agwat.2023.108183.

Allen, R.G., Jensen, M.E., Wright, J.L., Burman, R.D., 1989. Operational estimates of reference evapotranspiration. Agron. J. 81, 650–662. https://doi.org/10.2134/agronj1989.00021962008100040019x.

Arulampalam, M.S., Maskell, S., Gordon, N., Clapp, T., 2002. A tutorial on particle filters for online nonlinear/non-Gaussian Bayesian tracking. IEEE Trans. Signal Process. 50, 174–188. https://doi.org/10.1109/78.978374.

Baeza, P., Sánchez-de-Miguel, P., Centeno, A., Junquera, P., Linares, R., Lissarrague, J.R., 2007. Water relations between leaf water potential, photosynthesis and agronomic vine response as a tool for establishing thresholds in irrigation scheduling. Sci. Hortic. 114, 151–158. https://doi.org/10.1016/j.scienta.2007.06.012.

Baralon, K., Payan, J.-C., Salançon, E., Tisseyre, B., 2012. Spider: spatial extrapolation of the vine water status at the whole denomination scale from a reference well. OENO One 46, 167–175. https://doi.org/10.20870/oeno-one.2012.46.3.1517.

Benkendorf, D.J., Schwartz, S.D., Cutler, D.R., Hawkins, C.P., 2023. Correcting for the effects of class imbalance improves the performance of machine-learning based species distribution models. Ecological Modelling 483, 110414. https://doi.org/10.1016/j.ecolmodel.2023.110414.

Brunel, G., Pichon, L., Taylor, J., Tisseyre, B., 2019. Easy water stress detection system for vineyard irrigation management. in: Precision Agriculture ?19. Wageningen Academic Publishers, pp. 935–942. https://doi.org/10.3920/978-90-8686-888-9_115.

Celette, F., Ripoche, A., Gary, C., 2010. WaLIS—A simple model to simulate water partitioning in a crop association: The example of an intercropped vineyard. Agric. Water Manag. 97, 1749–1759. https://doi.org/10.1016/j.agwat.2010.06.008.

Chang, J., Bai, Y., Xue, J., Gong, L., Zeng, F., Sun, H., Hu, Y., Huang, H., Ma, Y., 2023. Dynamic Bayesian networks with application in environmental modeling and management: a review. Environ. Model. Softw. 170, 105835 https://doi.org/10.1016/j.envsoft.2023.105835.

Choné, X., Leeuwen, Van, Dubourdieu, C., Gaudillère, J.P, D., 2001. Stem water potential is a sensitive indicator of grapevine water status. Ann. Bot. 87, 477–483 https://doi.org/10.1006/anbo.2000.1361.

R. Core Team, 2021. R: A Language and Environment for Statistical Computing.

Deloire, A., Pellegrino, A., Rogiers, S., 2020. A few words on grapevine leaf water potential: Original language of the article: english. IVES Tech. Rev., vine wine. https://doi.org/10.20870/IVES-TR.2020.3620.

Destrac-Irvine, A., Van Leeuwen, K., 2018. VitAdapt, an Experimental Program to Study the Behavior of a Wide Range of Grape Varieties of Vitis vinifera in a Context of Climate Change in the Bordeaux Vineyards [WWW Document]. URL https://hal.archives-ouvertes.fr/ hal-03179912 (accessed 7.1.24).

Diago, M.P., Tardaguila, J., Barrio, I., Fernández-Novales, J., 2022. Combination of multispectral imagery, environmental data and thermography for on-the-go monitoring of the grapevine water status in commercial vineyards. Eur. J. Agron. 140, 126586 https://doi.org/10.1016/j.eja.2022.126586.

García-Tejera, O., López-Bernal, Á., Orgaz, F., Testi, L., Villalobos, F.J., 2021. The pitfalls of water potential for irrigation scheduling. Agric. Water Manag. 243, 106522 https://doi.org/10.1016/j.agwat.2020.106522.

Giovenzana, V., Beghi, R., Parisi, S., Brancadoro, L., Guidetti, R., 2018. Potential effectiveness of visible and near infrared spectroscopy coupled with wavelength

selection for real time grapevine leaf water status measurement. J. Sci. Food Agric. 98, 1935–1943. https://doi.org/10.1002/jsfa.8676.

Gordon, N.J., Salmond, D.J., Smith, A.F.M., 1993. Novel approach to nonlinear/non-Gaussian Bayesian state estimation. IEE Proc. F. (Radar Signal Process.) 140, 107–113. https://doi.org/10.1049/ip-f-2.1993.0015.

Keller, M., 2005. Deficit irrigation and vine mineral nutrition. Am. J. Enol. Vitic. 56, 267–283. https://doi.org/10.5344/ajev.2005.56.3.267.

Khanal, A.R., Mishra, A.K., Lambert, D.M., Paudel, K.P., 2019. Modeling post adoption decision in precision agriculture: a Bayesian approach. Comput. Electron. Agric. 162, 466–474. https://doi.org/10.1016/j.compag.2019.04.025.

Kocian, A., Massa, D., Cannazzaro, S., Incrocci, L., Di Lonardo, S., Milazzo, P., Chessa, S., 2020. Dynamic Bayesian network for crop growth prediction in greenhouses. Comput. Electron. Agric. 169, 105167 https://doi.org/10.1016/j.compag.2019.105167.

Kuhn, M., Johnson, K., 2013. Applied Predictive Modeling. In: Kuhn, M., Johnson, K. (Eds.), Applied Predictive Modeling. Springer, New York, NY, pp. 1–16. https://doi.org/10.1007/978-1-4614-6849-3_1.

Kuptametee, C., Aunsri, N., 2022. A review of resampling techniques in particle filtering framework. Measurement 193, 110836. https://doi.org/10.1016/j.measurement.2022.110836.

Laurent, C., Oger, B., Taylor, J.A., Scholasch, T., Metay, A., Tisseyre, B., 2021. A review of the issues, methods and perspectives for yield estimation, prediction and forecasting in viticulture. Eur. J. Agron. 130, 126339 https://doi.org/10.1016/j.eja.2021.126339.

Lebon, E., Dumas, V., Pieri, P., Schultz, H.R., 2003. Modelling the seasonal dynamics of the soil water balance of vineyards. Funct. Plant Biol. 30, 699–710. https://doi.org/10.1071/fp02222.

Lebon, E., Pellegrino, A., Louarn, G., Lecoeur, J., 2006. Branch Development Controls Leaf Area Dynamics in Grapevine (Vitis vinifera) Growing in Drying Soil. Ann. Bot. 98, 175–185. https://doi.org/10.1093/aob/mcl085.

Leeuwen, C., van, Trégoat, O., Choné, X., Bois, B., Pernet, D., Gaudillère, J.-P., 2009. Vine water status is a key factor in grape ripening and vintage quality for red Bordeaux wine. How can it be assessed for vineyard management purposes? OENO One 43, 121–134. https://doi.org/10.20870/oeno-one.2009.43.3.798.

Levin, A.D., 2019. Re-evaluating pressure chamber methods of water status determination in field-grown grapevine (Vitis spp.). Agric. Water Manag. 221, 422–429. https://doi.org/10.1016/j.agwat.2019.03.026.

Liaw, A., Wiener, M., 2002. Classification and regression by randomForest. R. N. 18–22.

Linde, N., Ginsbourger, D., Irving, J., Nobile, F., Doucet, A., 2017. On uncertainty quantification in hydrogeology and hydrogeophysics. Adv. Water Resour. 110, 166–181. https://doi.org/10.1016/j.advwatres.2017.10.014.

Luterbacher, J., García-Herrera, R., Akcer-On, S., Allan, R., Alvarez-Castro, M.-C., Benito, G., Booth, J., Büntgen, U., Cagatay, N., Colombaroli, D., Davis, B., Esper, J., Felis, T., Fleitmann, D., Frank, D., Gallego, D., Garcia-Bustamante, E., Glaser, R., Gonzalez-Rouco, F.J., Goosse, H., Kiefer, T., Macklin, M.G., Manning, S.W., Montagna, P., Newman, L., Power, M.J., Rath, V., Ribera, P., Riemann, D., Roberts, N., Sicre, M.-A., Silenzi, S., Tinner, W., Tzedakis, P.C., Valero-Garcés, B., van der Schrier, G., Vannière, B., Vogt, S., Wanner, H., Werner, J.P., Willett, G., Williams, M.H., Xoplaki, E., Zerefos, C.S., Zorita, E., 2012. 2 - A review of 2000 years of paleoclimatic evidence in the mediterranean. In: Lionello, P. (Ed.), The Climate of the Mediterranean Region. Elsevier, Oxford, pp. 87–185. https://doi.org/10.1016/B978-0-12-416042-2.00002-1.

McElreath, R., 2016. Statistical Rethinking: A Bayesian Course with Examples in R and Stan. Chapman and Hall/CRC, New York. https://doi.org/10.1201/9781315372495.

Meinshausen, N., 2006. Quantile regression forests. Journal of Machine Learning Research 983–999.

Montzka, C., Moradkhani, H., Weihermüller, L., Franssen, H.-J.H., Canty, M., Vereecken, H., 2011. Hydraulic parameter estimation by remotely-sensed top soil moisture observations with the particle filter. J. Hydrol. 399, 410–421. https://doi.org/10.1016/j.jhydrol.2011.01.020.

Pellegrino, A., Gozé, E., Lebon, E., Wery, J., 2006. A model-based diagnosis tool to evaluate the water stress experienced by grapevine in field sites. Eur. J. Agron. 25, 49–59. https://doi.org/10.1016/j.eja.2006.03.003.

Pellegrino, A., Lebon, E., Simonneau, T., Wery, J., 2005. Towards a simple indicator of water stress in grapevine (Vitis vinifera L.) based on the differential sensitivities of vegetative growth components. Aust. J. Grape Wine Res. 11, 306–315. https://doi.org/10.1111/j.1755-0238.2005.tb00030.x.

Pichon, L., Bopp, O., Tisseyre, B., 2021. 20. Characterising within-field variability of vine water status with simple visual observations of shoot growth. in: Precision Agriculture '21. Wageningen Academic Publishers, pp. 179–186. https://doi.org/10.3920/978-90-8686-916-9_20.

Pichon, Leo, Brunel, G., Payan, J.C., Taylor, J., Bellon-Maurel, V., Tisseyre, B., 2021. ApeX-Vigne: experiences in monitoring vine water status from within-field to regional scales using crowdsourcing data from a free mobile phone application. Precis. Agric. 22, 608. https://doi.org/10.1007/s11119-021-09797-9.

Pichon, L., Laurent, C., Payan, J.-C., Tisseyre, B., 2023. Observation of shoot growth: a simple and operational decision-making tool for monitoring vine water status in the vineyard. OENO One 57, 235–244. https://doi.org/10.20870/oeno-one.2023.57.1.5481.

Pôças, I., Rodrigues, A., Gonçalves, S., Costa, P.M., Gonçalves, I., Pereira, L.S., Cunha, M., 2015. Predicting grapevine water status based on hyperspectral reflectance vegetation indices. Remote Sens. 7, 16460–16479. https://doi.org/10.3390/rs71215835.

Pôças, I., Tosin, R., Gonçalves, I., Cunha, M., 2020. Toward a generalized predictive model of grapevine water status in Douro region from hyperspectral data. Agric. For. Meteorol. 280, 107793 https://doi.org/10.1016/j.agrformet.2019.107793.

Rienth, M., Scholasch, T., 2019. State-of-the-art of tools and methods to assess vine water status. OENO One 53. https://doi.org/10.20870/oeno-one.2019.53.4.2403.

Román Dobarco, M., Bourennane, H., Arrouays, D., Saby, N.P.A., Cousin, I., Martin, M.P., 2019. Uncertainty assessment of GlobalSoilMap soil available water capacity products: a French case study. Geoderma 344, 14–30. https://doi.org/10.1016/j.geoderma.2019.02.036.

Romero, M., Luo, Y., Su, B., Fuentes, S., 2018. Vineyard water status estimation using multispectral imagery from an UAV platform and machine learning algorithms for irrigation scheduling management. Comput. Electron. Agric. 147, 109–117. https://doi.org/10.1016/j.compag.2018.02.013.

Roux, S., Brun, F., Wallach, D., 2014. Combining input uncertainty and residual error in crop model predictions: a case study on vineyards. Eur. J. Agron. 52, 191–197. https://doi.org/10.1016/j.eja.2013.09.008.

Roux, S., Gaudin, R., Tisseyre, B., 2019. Why does spatial extrapolation of the vine water status make sense? Insights from a modelling approach. Agric. Water Manag. 217, 255. https://doi.org/10.1016/j.agwat.2019.03.013.

Scholander, P.F., Bradstreet, E.D., Hemmingsen, E.A., Hammel, H.T., 1965. Sap Pressure in Vascular Plants. Science 148, 339–346. https://doi.org/10.1126/science.148.3668.339.

Sun, Y., Kamel, M.S., Wong, A.K.C., Wang, Y., 2007. Cost-sensitive boosting for classification of imbalanced data. Pattern Recognit. 40, 3358–3378. https://doi.org/10.1016/j.patcog.2007.04.009.

Taylor, J.A., Acevedo-Opazo, C., Pellegrino, A., Ojeda, H., Tisseyre, B., 2012. Can within-season grapevine predawn leaf water potentials be predicted from meteorological data in non-irrigated Mediterranean vineyards? OENO One 46, 221–232. https://doi.org/10.20870/oeno-one.2012.46.3.1521.

Tosin, R., Martins, R., Pôças, I., Cunha, M., 2022. Canopy VIS-NIR spectroscopy and self-learning artificial intelligence for a generalised model of predawn leaf water potential in Vitis vinifera. Biosyst. Eng. 219, 235–258. https://doi.org/10.1016/j.biosystemseng.2022.05.007.

Tosin, R., Pôças, I., Novo, H., Teixeira, J., Fontes, N., Graça, A., Cunha, M., 2021. Assessing predawn leaf water potential based on hyperspectral data and pigment's concentration of Vitis vinifera L. in the Douro Wine Region. Sci. Hortic. 278, 109860 https://doi.org/10.1016/j.scienta.2020.109860.

Tuccio, L., Lo Piccolo, E., Battelli, R., Matteoli, S., Massai, R., Scalabrelli, G., Remorini, D., 2019. Physiological indicators to assess water status in potted grapevine (Vitis vinifera L.). Sci. Hortic. 255, 8–13. https://doi.org/10.1016/j.scienta.2019.05.017.

Wallach, D., Makowski, D., Jones, J.W., Brun, F., 2014. Chapter 1 - Basics of Agricultural System Models. In: Wallach, D., Makowski, D., Jones, J.W., Brun, F. (Eds.), Working with Dynamic Crop Models (Second Edition). Academic Press, San Diego, pp. 3–44. https://doi.org/10.1016/B978-0-12-397008-4.00001-0.

Winkler, A., Cook, J., Kliewer, W., Lider, L., 1974. General viticulture. University of California press, Berlekey, p. 710.

Xi, Z., Zhang, Z., Cheng, Y., Li, H., 2010. The effect of vineyard cover crop on main monomeric phenols of grape berry and wine in vitis viniferal L. cv. cabernet sauvignon. Agric. Sci. China 9, 440–448. https://doi.org/10.1016/S1671-2927(09)60115-2.